To appear in *Inverse Problems in Science and Engineering*
Vol. 00, No. 00, Month 20XX, 1–13

Inversion Methods for Laser Parameter Extraction with Phenomenological Model Based on Off-Axis Sensor Measurements

V. Kukreja[1*], N.D. Moshman[2], S. S. Sritharan[1], and J. DeGrassie[3]

[1] *Center for Decision, Risk, Controls & Signals Intelligence, Naval Postgraduate School, 1 University Circle, Monterey, CA, USA*; [2] *Applied Research Associates, 735 State St. Suite 516, Santa Barbara, CA, USA*; [3] *Atmospheric Propagation Branch, SPAWAR Systems Center Pacific, San Diego, CA, USA*

(*released July 2014*)

There are a wide range of applications involving laser propagation through a scattering medium. Very often, a measurement of the scattered light will be taken with the intent of learning some information about the medium. On the contrary, the present work seeks to extract a description of the source of light and its location. A phenomenological model for off-axis intensity is presented which employs a Mie scattering aerosol database. The model is extended to predict the off-axis polarized light described by the Stokes vector. Several inversion techniques are given and analyzed as well as example problems detailed which can recover the range, direction, power and polarization of the laser source.

Keywords: (High energy lasers, Laser parameter extraction, Mie scattering, Stokes vector, Laser beam polarization)

AMS Subject Classification: 49N45; 65Z05; 65K05.

Index to information contained in this guide

1. Introduction

High energy lasers (HELs) as directed energy weapons are increasingly becoming present in defense applications. In the future, HELs weapon systems are to be deployed on various platforms in the sea, air as well as ground based devices to attack targets and conduct operations over several kilometers. To counter these weapons, specifically to provide warning and enact counter-measures, it will be important to identify the threat laser power and location as well as the laser beam direction. As such, a reliable and robust

*Corresponding author. Email: vkukreja@nps.edu

model is needed to predict HELs power level and characterize HELs from an off-axis site.

Earlier works have shown that laser beams can be detected from the photons scattered off the aerosols in the beam path. Particularly, the measured intensity of scattered light is in good agreement with the prediction from Mie scattering theory [2]. Further studies have concluded that various environmental factors can affect the aerosol distribution modeling [3]. Specifically, when humidity is increased, the scattering becomes stronger due to the presence of larger aerosols in the atmosphere ([4], [5]). In [6], a phenomenological model for remote detection of scattered light is presented and compared with experimental intensity measurements. Furthermore, the model in [6] is tested against a range of aerosol distributions present in the atmosphere under different weather conditions. We refer to [6] for complete details on the experiment and the comparison of experimental data with the model predictions for the scattered light (see Figures 5 and 6 in [6]).

Given a volume scattering function, it is noted in [6] that the scattered intensity at the receiver is affected by the laser power as well as the source distance and direction, and often the laser parameters cannot be uniquely determined from only the intensity measurements. In [6], it is observed experimentally that even if the beam location is known, the laser power level and direction still cannot be resolved. To solve this problem, accurate timing of the received intensity is taken in the experiment to estimate the laser direction and consequently beam power level. In this paper, we devise and analyze several inversion methods to solve the laser parameter extraction problem for the phenomenological model in [6]. Based on only simulated intensity measurements, the inversion algorithms we have constructed can uniquely solve for any single unknown parameter. The limitations of each method vary as the number of unknowns increases. All methods fail to find a unique solution when all four parameters in the phenomenological model are unknown. The capability of sensors to measure polarized light and the capability of the Advance Navy Aerosol Model (ANAM) to model polarized aerosol scattering motivated an extension of the phenomenological model to the Stokes vector for polarized light undergoing Mie scattering. When polarization of light is incorporated, four unknown parameters can be uniquely determined.

We further remark that, in the analysis of the scalar radiative transfer equation for un-polarized light, it has been noted in [7, 8] that, in the steady state case, neglecting the polarization of light can lead to significant error for the total intensity. It would be interesting to clarify the connection between the extended phenomenological model in this work and the radiative transfer equations [9, 10], and compare the full impact of the degree of the polarization on the off-axis intensity measurements of scattered light and consequently on the values to which the inversion algorithms converge for the laser parameters. Nonetheless, the results presented in this paper illustrate how Mie scattering polarizes light, and that including polarization is fundamental to accurately model the state of light as the laser beam scatters off aerosols in the atmosphere.

2. Phenomenological Models

In this section, we formulate the necessary mathematical models in connection with the laser parameters inversion problem for the scalar intensity equation and the extension of this equation including the Stokes vector for polarized light.

2.1 *Off-Axis Intensity Model*

A phenomenological model (cf. [6]) for electromagnetic intensity given off by a laser source in two-dimensional (2D) space is given as:

$$I_j = \int_{\theta_{min}}^{\theta_{max}} P_0 \cdot e^{-\alpha(z+r)} \frac{\beta(\theta' + \psi)}{Rsin\psi} d\theta' \tag{1}$$

It is assumed that the light scatters only once, a distance z from the source, and travels a distance r to a receiver. The receiver is located a distance R from the source. These three distances uniquely define a triangle. The beam power at the source is P_0. The angle ψ, the 'source' or 'beam' angle is the angle between the direction of light propagation from the source and the direction from source to receiver. The angle θ, the 'viewing angle', is the angle between the direction from the receiver to the scattering site and the receiver to the source. The problem geometry is shown in Figure 1. In the limits of the integral, $\theta_{max} = \theta + \Delta\theta/2$ and $\theta_{min} = \theta - \Delta\theta/2$ where the intensity I_j is the intensity at $\theta = 3°$ in the center of the angular range $\Delta\theta$ of the receiver in the scattering plane. The receiver collects the scattered light and records the intensity over a horizontal field of view (FOV).

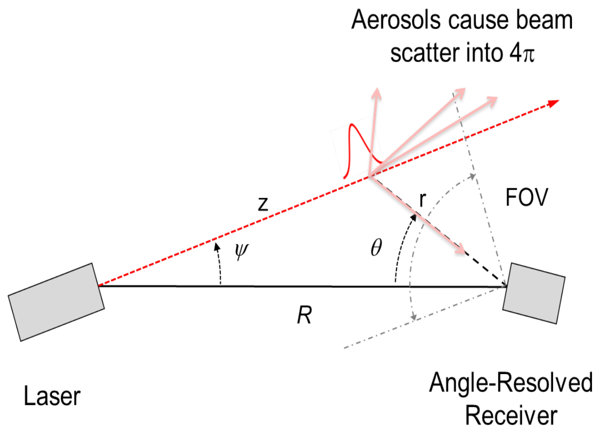

Figure 1.: Diagram of beam path from source to receiver.

The extinction coefficient α (km^{-1}) gives the rate of intensity loss per distance traveled along the beam. The scattering coefficient $\beta = \beta(\psi + \theta)$ $(km^{-1}sr^{-1})$ gives the amount of radiation scattered in a particular direction. Both of these quantities are dependent on the local atmospheric properties. The ANAM code ([11],[12]) is used to generate explicit values of α and β for a given location with certain meteorological conditions.

Equation (1) is derived in [6] under certain additional physical assumptions: 1) the medium is uniform and homogeneous, 2) the beam is one-dimensional (beam size and divergence are neglected) as the size-scale of detection is over several kilometers, 3) multiple scattering events are neglected since the mean free path $1/b$ is large compared to the receiver distance R to the laser source (here, total scattering $b = \frac{1}{2\pi}\int_0^{\pi} sin(\theta)\beta(\theta)d\theta$), and 4) the ratio of beam width to the propagation time along the path from the source to receiver is large (the long-pulse limit). We refer to [6] for the complete derivation of equation (1) and further discussion of off-axis scattering theory for free-space lasers.

Assuming that scattering parameters are known, intensity at the receiver depends on the six variables $\{P_0, z, r, R, \psi, \theta\}$. However, since there are geometric constraints, two of the the unknowns will be fixed by some arrangement of the law of cosines and the law of sines.

$$\begin{aligned} &R = z \cdot cos\psi + \sqrt{(z \cdot cos\psi)^2 - (z^2 - r^2)} \\ &\psi = sin^{-1}\left(\tfrac{r \cdot sin\theta}{z}\right) \end{aligned} \tag{2}$$

2.2 *Off-Axis Polarization Model*

Assuming that aerosols in the atmosphere are reasonably far from each other and the distance between the particles is much greater than the laser wavelength, then the type of scattering which occurs is called *independent scattering* (see [1] for more details). This is a reasonable model to study scattering for the types of aerosols of interest. An elliptically polarized state of light can be uniquely described by the Stokes vector [9]. An analogous extension of the phenomenological model of intensity after scattering is as follows. The scalar state equation, (1), becomes a vector of four components which, as a whole, uniquely determine the elliptical parameters of the polarization state.

$$I \rightarrow (I, Q, U, V) \tag{3}$$

The volume scattering coefficient β becomes a 4-by-4 matrix, $\tilde{S}$, which is the product of a scattering matrix, S, and linear rotation matrices between the meridian planes of the source and receiver with the scattering plane.

$$\beta \rightarrow \tilde{S} = T(-\phi_1) \cdot S \cdot T(-\phi_2) \tag{4}$$

S is the Mie Scattering Matrix. The individual elements s_{ij} depend on the scattering angle and are given by ANAM.

$$S = \begin{pmatrix} s_{11} & s_{12} & 0 & 0 \\ s_{12} & s_{11} & 0 & 0 \\ 0 & 0 & s_{33} & s_{34} \\ 0 & 0 & -s_{34} & s_{33} \end{pmatrix} \tag{5}$$

The linear transformation matrix, $T(\phi)$, is defined below.

$$T(\phi) = \begin{pmatrix} 1 & 0 & 0 & 0 \\ 0 & cos(-2\phi) & -sin(-2\phi) & 0 \\ 0 & sin(-2\phi) & cos(-2\phi) & 0 \\ 0 & 0 & 0 & 1 \end{pmatrix} \tag{6}$$

Assuming a 2D geometry implies that the rotation angles ϕ_1 and ϕ_2 both have magnitude $\frac{\pi}{2}$, as shown in Figure 2a. In the case of 3D geometry shown in Figure 2b, the elevation angle would be an additional unknown. The extended off-axis phenomenological polarized scattering model is given in equation (7).

$$(I,Q,U,V)^T(\theta) = \int_{\theta_{min}}^{\theta_{max}} \frac{e^{-\alpha(z+r)}}{Rsin\psi} \cdot \tilde{S}(\theta' + \psi) \cdot (I_0, Q_0, U_0, V_0)^T(\theta') d\theta' \tag{7}$$

Incident light that is purely elliptically polarized will also obey equation (8).

$$I_0^2 = Q_0^2 + U_0^2 + V_0^2 \tag{8}$$

After scattering, the light can have a polarized component and non-polarized component. The fraction of the scattered light that remains polarized is also called the degree of polarization (DOP), given in equation (9). In the results section it will be shown that the type of incident polarization fixes the how the degree of polarization varies with scattering angle.

$$DOP = \frac{\sqrt{Q^2 + U^2 + V^2}}{I} \tag{9}$$

3. Inverse Problem Formulation

3.1 *Mayer-type Problem*

The essence of a Mayer formulation is to minimize the difference between a final state and measured data, given a model of how the state is constrained to evolve. In this case, the unknown is the initial data. For the scalar problem, equation (1) is the state model and the system must also obey the geometric constraints in equation (2). For the vector problem, equation (7) is the state model, the geometric constraints still apply and the incident Stokes vector will also obey equation (8). All of the scattering information comes from ANAM and can be assumed as known.

The objective functional to be minimized in the Mayer formulation is given in equation (10). The quantity L_j represents the integrand of equation (1). Notice that if L_j is correct at each viewing angle, then the intensity will be correct. Physically this is analogous to modeling the radiance which has units of intensity per solid angle, $\frac{W}{m^2 \cdot sr}$, but since the problem is planar 2D geometry, the units are in fact $\frac{W}{m^2 \cdot rad}$. The discrete set of measured data at N different viewing angles is denoted as $M = (m_1, m_2, \ldots, m_N)$.

$$J = \frac{1}{2} \sum_{j=1}^{N} (L_j - m_j)^2 \tag{10}$$

An optimal solution must also satisfy the differential constraints along the beam. By inspection of equation (1), it is seen that $\frac{\partial L_j}{\partial r} = \frac{\partial L_j}{\partial z} = -\alpha L_j$. By adjoining these constraints with lagrange multipliers, the augmented cost functional is defined in equation (11).

$$\tilde{J}(z,r) = \frac{1}{2}\sum_{j=1}^{N}(L_j - m_j)^2 + \int_0^{z_0} \lambda_z \cdot \left(\frac{\partial L_j}{\partial z} + \alpha L_j\right) dz + \int_0^{r_0} \lambda_r \cdot \left(\frac{\partial L_j}{\partial r} + \alpha L_j\right) dr \quad (11)$$

Optimal conditions are found by calculating the following derivative. Let ϵ be a small positive constant. The variational terms are undetermined.

$$\frac{d}{d\epsilon}\tilde{J}(z_0 + \epsilon\delta z, r_0 + \epsilon\delta r)|_{\epsilon=0} = 0 \quad (12)$$

Therefore,

$$\begin{aligned}
&0 = \tfrac{1}{2}\textstyle\sum_{j=1}^{N} \tfrac{d}{d\epsilon}\left[(L_j(z+\epsilon\delta z, r+\epsilon\delta r) - m_j)^2\right]_{\epsilon=0} + \\
&\tfrac{d}{d\epsilon}\textstyle\int_0^{z_0}(\lambda_z + \epsilon\delta\lambda z)\cdot\left(\tfrac{\partial L_j}{\partial z}(z+\epsilon\delta z, r+\epsilon\delta r) + \alpha L_j(z+\epsilon\delta z, r+\epsilon\delta r)\right)_{\epsilon=0} dz + \\
&\tfrac{d}{d\epsilon}\textstyle\int_0^{r_0}(\lambda_r + \epsilon\delta\lambda r)\cdot\left(\tfrac{\partial L_j}{\partial r}(z+\epsilon\delta z, r+\epsilon\delta r) + \alpha L_j(z+\epsilon\delta z, r+\epsilon\delta r)\right)_{\epsilon=0} dr
\end{aligned} \quad (13)$$

Look at the three terms separately.

The first term K_1:

$$\begin{aligned}
&K_1 = \tfrac{1}{2}\textstyle\sum_{j=1}^{N}\left[(L_j(z+\epsilon\delta z, r+\epsilon\delta r) - m_j)\cdot\tfrac{d}{d\epsilon}L_j(z+\epsilon\delta z, r+\epsilon\delta r)\right]_{\epsilon=0} \\
&= \tfrac{1}{2}\textstyle\sum_{j=1}^{N}(L_j(z,r) - m_j)\cdot\delta L_j
\end{aligned} \quad (14)$$

The second term K_2:

$$\begin{aligned}
&K_2 = \textstyle\int_0^{z_0}\delta\lambda_z\cdot\left(\tfrac{\partial L_j}{\partial z}(z+\epsilon\delta z, r+\epsilon\delta r) + \alpha L_j(z+\epsilon\delta z, r+\epsilon\delta r)\right)_{\epsilon=0} + \\
&(\lambda_z + \epsilon\delta\lambda_z)\left(\tfrac{\partial}{\partial z}\tfrac{d}{d\epsilon}L_j(z+\epsilon\delta z, r+\epsilon\delta r) + \alpha\tfrac{d}{d\epsilon}L_j(z+\epsilon\delta z, r+\epsilon\delta r)\right)_{\epsilon=0} dz \\
&= \textstyle\int_0^{z_0}\delta\lambda_z\cdot\left(\tfrac{\partial L_j}{\partial z}(z,r) + \alpha L_j(z,r)\right) + \lambda_z\cdot\left(\tfrac{\partial}{\partial z}\delta L_j + \alpha\delta L_j\right) dz \\
&= [\lambda_z\cdot\delta L_j]_0^{z_0} + \textstyle\int_0^{z_0}\delta\lambda_z\cdot\left(\tfrac{\partial L_j}{\partial z}(z,r) + \alpha L_j(z,r)\right) + \left(-\tfrac{\partial\lambda_z}{\partial z}\cdot\delta L_j + \lambda_z\alpha\delta L_j\right) dz
\end{aligned} \quad (15)$$

And similarly for the third term K_3:

$$\begin{aligned}
&K_3 = \textstyle\int_0^{r_0}\delta\lambda_r\cdot\left(\tfrac{\partial L_j}{\partial r}(z+\epsilon\delta z, r+\epsilon\delta r) + \alpha L_j(z+\epsilon\delta z, r+\epsilon\delta r)\right)_{\epsilon=0} + \\
&(\lambda_r + \epsilon\delta\lambda_r)\left(\tfrac{\partial}{\partial r}\tfrac{d}{d\epsilon}L_j(z+\epsilon\delta z, r+\epsilon\delta r) + \alpha\tfrac{d}{d\epsilon}L_j(z+\epsilon\delta z, r+\epsilon\delta r)\right)_{\epsilon=0} dr \\
&= \textstyle\int_0^{r_0}\delta\lambda_r\cdot\left(\tfrac{\partial L_j}{\partial r}(z,r) + \alpha L_j(z,r)\right) + \lambda_r\cdot\left(\tfrac{\partial}{\partial r}\delta L_j + \alpha\delta L_j\right) dr \\
&= [\lambda_r\cdot\delta L_j]_0^{r_0} + \textstyle\int_0^{r_0}\delta\lambda_r\cdot\left(\tfrac{\partial L_j}{\partial r}(z,r) + \alpha L_j(z,r)\right) + \left(-\tfrac{\partial\lambda_r}{\partial r}\cdot\delta L_j + \lambda_r\alpha\delta L_j\right) dr
\end{aligned} \quad (16)$$

Putting it all together gives:

$$\begin{aligned}
&0 = \tfrac{1}{2}\textstyle\sum_{j=1}^{N}(L_j(z,r) - m_j)\cdot \delta L_j + \\
&[\lambda_z \cdot \delta L_j]_0^{z_0} + \textstyle\int_0^{z_0} \delta\lambda_z \cdot \left(\tfrac{\partial L_j}{\partial z}(z,r) + \alpha L_j(z,r)\right) + \delta L_j \cdot \left(-\tfrac{\partial \lambda_z}{\partial z} + \lambda_z\alpha\right) dz + \\
&[\lambda_r \cdot \delta L_j]_0^{r_0} + \textstyle\int_0^{r_0} \delta\lambda_r \cdot \left(\tfrac{\partial L_j}{\partial r}(z,r) + \alpha L_j(z,r)\right) + \delta L_j \cdot \left(-\tfrac{\partial \lambda_r}{\partial r} + \lambda_r\alpha\right) dr
\end{aligned} \tag{17}$$

The terms that are multiplying $\delta\lambda_z$ and $\delta\lambda_r$ are just the state equations. Grouping what remains will give the adjoint differential equations and boundary conditions.

Boundary Conditions:

$$\begin{aligned}
&0 = (L_j(z_0,r_0) - M)\cdot \delta L_j(z_0,r_0) + \\
&(\lambda_z(z_0)\delta L_j(z_0,0) - \lambda_z(0)\delta L_j(0,0)) + \\
&(\lambda_r(r_0)\delta L_j(z_0,r_0) - \lambda_r(0)\delta L_j(z_0,0))
\end{aligned} \tag{18}$$

Grouping like terms gives:

$$\begin{aligned}
&\lambda_r(r_0) = -(L_j(z_0,r_0) - m_j) \\
&\lambda_z(z_0) = \lambda_r(0) \\
&\lambda_z(0)\cdot \delta L_j(0,0) = 0
\end{aligned} \tag{19}$$

Going back to Equation (17), the adjoint differential equations, after canceling out the δL_j multiplier, are:

$$\begin{aligned}
&\textstyle\int_0^{r_0} \left(\tfrac{\partial \lambda_r}{\partial r} - \alpha\lambda_r\right) dr = 0 \\
&\textstyle\int_0^{z_0} \left(\tfrac{\partial \lambda_z}{\partial z} - \alpha\lambda_z\right) dz = 0
\end{aligned} \tag{20}$$

3.2 *Parameter Expansion*

The second approach treats equation (1) as a nonlinear map, G, from a space of unknown parameters, $x = (P_0, R, \theta_j, \psi)$, to a set of measurements M. Let the set of true values of the parameters be defined as x_0. Then the nonlinear map will satisfy equation (21).

$$G(x_0) = M \tag{21}$$

Taking a small variation δx from the true parameters, the Taylor expansion of the map truncated after the first term is shown in equation (22).

$$G(x_0 + \delta x) = G(x_0) + G'(x_0)\cdot \delta x + ... \tag{22}$$

The left hand side of Equation (22) will yield a prediction of the data, I_{calc}, that is not the true measured data M. Further manipulation will give a search direction (δx) for the parameters based on the error ($I_{calc} - M$).

$$
\begin{aligned}
I_{calc} &= M + G'(x_0) \cdot \delta x \\
I_{calc} - M &= G'(x_0) \cdot \delta x \\
(G')^T(I_{calc} - M) &= (G')^T G'(x_0) \cdot \delta x \\
\delta x &= [(G')^T G']^{-1} (G')^T (x_0)(I_{calc} - M)
\end{aligned}
\tag{23}
$$

The derivative of the map is defined as $G' \equiv \frac{\partial I_{calc}}{\partial x}$. The terms are shown in equation (24).

$$
\begin{aligned}
\tfrac{\partial I_{calc}}{\partial P_0} &= \tfrac{I_{calc}}{P_0} \\
\tfrac{\partial I_{calc}}{\partial R} &= -I_{calc}\{\alpha \left(\tfrac{\partial z}{\partial R} + \tfrac{\partial r}{\partial R}\right) + \tfrac{1}{R}\} \\
\tfrac{\partial I_{calc}}{\partial \theta} &= -I_{calc}\{\alpha \left(\tfrac{\partial z}{\partial \theta} + \tfrac{\partial r}{\partial \theta}\right) - \tfrac{1}{\beta}\tfrac{\partial \beta}{\partial \theta}\} \\
\tfrac{\partial I_{calc}}{\partial \psi} &= -I_{calc}\{\alpha \left(\tfrac{\partial z}{\partial \psi} + \tfrac{\partial r}{\partial \psi}\right) - \tfrac{1}{\beta}\tfrac{\partial \beta}{\partial \psi} + cot(\psi)\}
\end{aligned}
\tag{24}
$$

The partial derivatives from equation (24) are defined in Equation (25).

$$
\begin{aligned}
\tfrac{\partial z}{\partial R} &= \tfrac{sin(\theta)}{sin(\theta+\psi)} \\
\tfrac{\partial z}{\partial \theta} &= \tfrac{r \cdot cos(\theta)}{sin(\psi)} \\
\tfrac{\partial z}{\partial \psi} &= \tfrac{-r \cdot sin(\theta) \cdot cos(\psi)}{sin(\psi)^2} \\
\tfrac{\partial r}{\partial R} &= \tfrac{sin(\psi)}{sin(\theta+\psi)} \\
\tfrac{\partial r}{\partial \theta} &= \tfrac{-z \cdot sin(\psi) \cdot cos(\theta)}{sin(\theta)^2} \\
\tfrac{\partial r}{\partial \psi} &= \tfrac{z \cdot cos(\psi)}{sin(\theta)}
\end{aligned}
\tag{25}
$$

In the polarization problem, the number of parameters increases from four to seven. The three additional unknowns come from the initial values of the Stokes vector.

$$
x = (I_0, Q_0, U_0, V_0, R, \theta, \psi) \tag{26}
$$

The map from parameter space to data measurement is extended to the Stokes vector in equation (27).

$$
G = k(\theta, \psi, R) \cdot \tilde{S}(\theta, \psi) \cdot (I_0, Q_0, U_0, V_0)^T \tag{27}
$$

$$
k = \frac{e^{-\alpha(z+r)}}{Rsin(\psi)} \tag{28}
$$

$$G : x_j \rightarrow (I_j, Q_j, U_j, V_j) \tag{29}$$

Let

$$\begin{aligned}\vec{I_0} &= (I_0, Q_0, U_0, V_0)^T \\ \vec{I_i} &= (I_i, Q_i, U_i, V_i)^T\end{aligned} \tag{30}$$

where $\vec{I_0}$ is the Stokes vector of the emitted light at the source and $\vec{I_j}$ is the j^{th} measurement of the Stokes vector, off-axis and downrange, at the viewing angle θ_j. The index j is the number of (4-component) measurements from a single, static sensor. Each can be distinguished by a different viewing angle θ_j which can be considered a known or single unknown parameter θ since all will be equally spaced. The index i is the parameter index which runs from 1 to 7 for all four stokes parameters, range, beam emission angle and sensor viewing angle.

As an example, equation (31) shows the derivative of the second parameter,Q_0, with respect to the fifth, R,

$$\frac{\partial Q}{\partial R} = \frac{\partial k}{\partial R} \cdot \tilde{S_{2l}}(\vec{I_0})_l \tag{31}$$

where the index l is summed over from 1 to 4.

4. Inversion Methods

4.1 *Shooting Algorithm*

(1) Assume known values for α, β and measurement M for a chosen set of viewing angles θ_j. Guess initial values for z_0 and r_0. These values will fix R and ψ from the geometric constraints.
(2) Solve for L_j at the receiver. There will be some non-zero difference between the calculated intensity and the measurement $L_j - m_j$.
(3) Use equation (19) for a boundary condition on $\lambda_r(r_0)$ and use equation (20) to integrate from the receiver to the scattering site to obtain a value for $\lambda_z(z_0)$.
(4) Again, use equation (20) to integrate from the scattering site to the source to get a value for $\lambda_z(0)$
(5) At the optimal solution, the boundary values on the co-states will be zero and, therefore, their integrals will remain zero. Hence, the non-zero values of $\lambda_z(0)$ and $\lambda_r(0)$ represent search directions for updates to the lengths r_0 and z_0.
(6) The new values of r_0 and z_0 with fix values for R and ψ, using Equation (2), such that the geometric constraints are obeyed.
(7) Repeat steps 2-6 until the value of L_j matches the measurement m_j.

Note: The solution to L_j will match the measurement at the chosen viewing angle but this solution is not unique. The slope of the result with respect to θ will still be free to vary. Consequently, performing this procedure using several chosen viewing angles will fix both the values and the slope of L_j resulting in a unique solution.

4.2 *Newton's Method*

(1) Assume known values for α, β and measurement set M for a chosen set of viewing angles θ.
(2) A set of parameters can be chosen as the unknowns and the rest are fixed at their true values.
(3) A set of intensities at each viewing angle are calculated. The difference between the calculated values and the actual measurements are then used in equation (23) to update the unknown parameters by determining the search direction. Note that a fixed step size is always taken in the search direction δx.
(4) The lengths z and r are updated from rearranging the geometric constraints in equation (2).
(5) Repeat steps 2-4 until the calculated intensity, I_{calc}, matches the measured intensity M.

4.3 *Simplex Method*

The simplex method, as it is used here, seeks to minimize the same objective functional as that of the Mayer formulation, equation (10). However, the simplex method is the only method presented which does not approximate first derivatives. Instead, a set of points in the parameter space and their resulting errors are stored. The evaluation of the error from a new point determines which in the set will be dropped and which kept. The size of the simplex contracts around a minimum until a tolerance in both the error and parameter step size is reached. There are many general purpose simplex methods available and in this work, MATLAB's 'fminsearch' was used.

5. Results and Analysis

Table 1 shows the ANAM input parameters for all of the results presented. In addition, for both scalar and vector results, the *runAngles* flag must be *true* and only for the vector cases is the *polarization* flag set to *true*.

5.1 *Shooting Method*

Figure 3a shows a result using the Mayer-type formulation and shooting method. Notice that the value and slope of the blue curves matches the trend in the measurements. Without multiple measurements, this method would fail. It was found that this method could solve the problem with certain combinations of up to two unknowns, but each different combination of unknowns requires a different arrangement of the geometric constraints and convergence was sensitive to the initial guess. Figure 3b shows convergence of the parameters to the true values, and the error down to machine precision. In this result, the unknown parameter is the range and the initial guess is off by 5% of the true value.

5.2 *Newton's Method*

The major advantage of Newton's Method over the Shooting Method is that the same procedure and equations are used regardless of which parameters are unknown. Figures 4-7 show results using Newton's Method. Figure 4 shows two cases where only one out of the four parameters is unknown. The true value of the unknown parameter is determined down to machine precision. In this section, the initial guess was within 25% of the true value.

Figure 5 shows two cases where two out of the four parameters are unknown. Once again, the true values of the unknown parameters are determined down to machine precision.

Figure 6 shows two cases where three out of the four parameters are unknown. Notice that in Figure 6.a, the errors in θ and ψ converge to a non-zero value while the cost functional still achieves a very small value. This shows a non-uniqueness in the phenomenological model to the quantity $\theta + \psi$ when three or more quantities are unknown. A similar result is shown in Figure 6.b to the error in the quantities R and P_0. This shows another non-uniqueness to the quantity $\frac{P_0}{R}$ when three or more quantities are unknown.

Figure 7 shows two cases where all four parameters are unknown. Figure 7.a is based on a cost functional with four measurements while Figure 7.b used six measurements.

Both of the non-uniquenesses are present in this result. With more measurements, the inversion algorithm calculates the values of $\theta + \psi$ and $\frac{P_0}{R}$ which get closer to the true values. Some of the non-uniqueness might be dealt with by using measurements that not only differ by viewing angle, but also by range and beam angle. This could be achieved by multiple sensors placed asymmetrically about the beam axis.

5.3 *Simplex Method*

All of the results in this section are for an initial power $P_0 = 100$ kW, range $R = 5$ km, beam angle $\psi = 30°$ and viewing angles $\{\theta_i\}_{i=1}^{5} = \{10°, 27.5°, 45°, 62.5°, 80°\}$. The initial guess for any unknown is within 25% of the true value.

The use of MATLAB's optimization tool **fminsearch** leads to better control in 'tuning' search direction limiters and makes the Matrix Inversion method more robust. We obtain far more efficient rates for convergence down to machine precision for one unknown parameter inversions (see Figures 8a-8b) and two unknown parameters inversions (see Figures 8c-8d). More importantly, the three unknown parameters inversion problem (see Figure 8e) is completely resolved. However, for the case in which all four free parameters are unknown, the method still converges to non-unique values (see Figure 8f). This inability to solve four unknown problem uniquely motivates the inclusion of polarization and the inversion of the vector problem.

Scattering can change the DOP of scattered light. For a given scattering kernel, the degree of polarization depends on two factors: 1) the initial polarization state and 2) the scattering angle. Elliptical representations of incident Stokes vectors are given in Figure 9a. Figures 9b-f show the scattered and attenuated ellipses for various types of incident polarization as a surface with the scattering angle as the z-axis.

The scattered Stokes vector components versus scattering angle for each incident polarization state are shown in Figures 10a-f. For each scattering angle, the solid curve for each Stokes component represent the magnitude of the component *without* attentuation (extinction rate $\alpha = 0\ km^{-1}$) and the corresponding dashed curve represent the magnitude of the component *with* attentuation (extinction rate $\alpha = 0.02\ km^{-1}$). Note that if one of the components is uniformly zero it will not appear on the logarithmic scale. By inspection, the Stokes components and the elliptical axes are minimum at about 120° scattering angle.

Figure 11 shows how the DOP changes with scattering angle for all of the types of incident polarization considered. Rayleigh scattering of unpolarized light is included to highlight the difference from the Mie model. It is interesting to note that linear vertical and horizontal polarization are the only types which remain fully polarized after Mie scattering. All fully-polarized light states remain so under Rayleigh scattering as well. The other four types of incident polarization follow the exact same trend under Mie scattering. At about 100° of scattering angle they are composed equally of polarized and unpolarized light.

Figures 12a-f shows results for the inversion of the Stokes vector (I_0, Q_0, U_0, V_0) with the beam geometry parameters (R, ψ, θ) for horizontally polarized light. Figures 11a and 11b show convergence down to machine precision for one unknown parameter I_0 and two unknowns parameters (I_0, Q_0), respectively. Figure 11c shows the inversion for the three unknown parameters case (I_0, R, ψ), verifying that the simplex method is robust enough to determine the laser power as well as beam location and angle for a polarized laser beam. Most importantly here, we finally obtain, as indicated in Figure 12d-f, the full inversion of all four parameters (I_0, R, ψ, θ) for a case of each of the DOP curves in Figure 11.

In an effort to make the results contained in this manuscript more useful in the less ideal real world, a simple noise study was conducted to quantify the robustness of the model and solution method. Two types of noise were considered; white noise at the sensor and uniform uncertainty in the meteorological inputs to ANAM for each beam path. Figures 13a-f show the results for white noise and Table 2 shows the results for meteorological uncertainty.

A normally distributed random variable with standard deviation scaled to the signal was added to each measurement. A sample size of 1000 was used for each trial with the simplex method. A histogram of the error of the resulting prediction for an unknown parameter is shown in Figure 13a. The error is normally distributed which justifies the use of confidence intervals of one standard deviation on each side of the true parameter value, which are shown in Figures 13b-e. The horizontal axis in Figures 13b-e is the log base 10 of the noise-to-signal ratio. As can be clearly seen, more unknowns make the confidence interval larger for the same amount of sensor noise. The noise levels were chosen such that the standard deviation of the error was between 0.1 and 1.

In addition, the ANAM meteorological input parameters were varied to assess the sensitivity of a unique solution to uncertainty in the scattering environment. Table 2 demonstrates that with up to 20% variation in ANAM input, the simplex method still recovers the right parameters to within about 1%. The noise study demonstrates that the simplex method presented will be predictably robust against sensor noise and that the sensitivity to ANAM input is small.

6. Conclusions

In the coming years, HELs will be in operation on many platforms on sea, land, and in the air. In response, advance warning systems and countermeasure operations will require a robust capability to detect and characterize laser sources from an off-axis location. Of the three inversion methods presented, the *simplex method* is by far the most reliable and complete approach to solve the nonlinear inverse problems.

Extension of the off-axis intensity model to include the scattering effects of polarized light was worthwhile since that proved to be the only way to uniquely determine three or more unknown parameters. The solvability of the four unknown problem using the Stokes model and simplex method was found to be insensitive to the incident polarization state.

Acknowledgments

The authors would like to thank MASINT and the Office of Naval Research for supporting this research, and SPAWAR Systems Pacific for providing the Navy's ANAM code. The authors also are grateful to Professor Guillaume Bal for helpful discussions.

References

[1] K.-N Liou, A complementary theory of light scattering by homogenous spheres. Applied Mathematics and Computation 3, 331–358 (1977).
[2] J.P. Cariou, Off-axis detection of pulsed laser beams: simulation and measurements in the lower atmosphere, Proc. SPIE 5086, 129–138 (2003).
[3] S. Doss-Hammel, Dimitri Tsintikidis, Dave Merritt, and Jim Fontana, Atmospheric characterization for high-energy laser beam propagation in the maritime environment, Proc. SPIE 5552, 208–219 (2004).
[4] N. Roy and F. Reid, Off-axis laser detection model in coastal areas, Opt. Eng. 47, 086002 (2008).
[5] J. K. Michuleu and R. Schleijpen, Influence of aerosols on off-axis laser detection capabilities, Proc. SPIE 7463, 1–12 (2009).
[6] F. Hanson, I. Bendall, C. Deckard, and H. Haider, Off-axis detection and characterization of laser beams in the maritime atmosphere. Applied Optics 50. 18, 3050–3056 (2011).
[7] M. I. Mishchenko and A. A. Lacis, Errors induced by the neglect of polarization in radiance calculations for Rayleigh-scattering atmospheres, JQSRT 51 (3), 391–510 (1994).
[8] A. Ambirajan and D. C. Look, A backward Monte Carlo study of multiple scattering of a polarized laser beam, JQSRT 58 (2), 171–192 (1997).
[9] S. Chandrasekhar, Radiative transfer, Cambridge: Oxford University Press, 1960.
[10] A. Ishimaru, Wave propagation and scattering in random media, New York: Academics, 1978.
[11] S.G. Gathman, Optical properties of the marine aerosol as predicted by the Navy aerosol model, Opt. Eng. 22, 57–62 (1983).
[12] S. Doss-Hammel, A. van Eijk, and D. Tsintikidis, ANAM vs. NAM: is the difference significant?, Proc. SPIE 5891, 1–12 (2005).

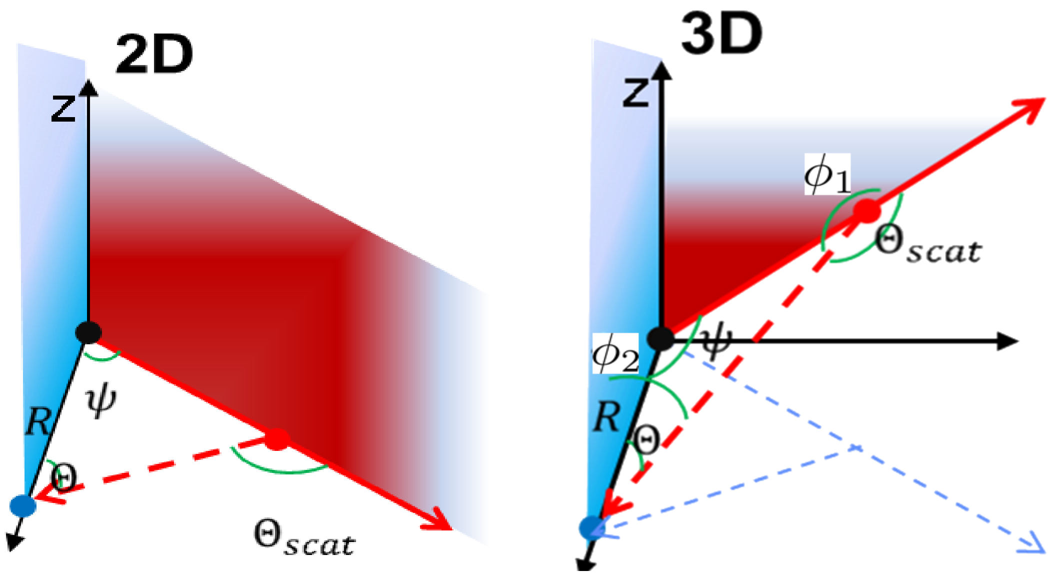

Figure 2.: (2.a) Problem geometry in two dimensions (2.b) Problem geometry in three dimensions

Quantity	Name	Value	Units
Laser Wavelength	λ	1.064	μm
Instantaneous Wind Speed	mets.u10	3	m/s
24-hr Average Wind Speed	mets.u24	8	m/s
Altitude	mets.z	2	m
Relative Humidity	mets.RH	40	%
Air Mass Parameter	mets.AMP	3	-
ANAM Version	modelchoice	anam4	-
Angular Resolution	angelRes	1	$^\circ$

Table 1.: ANAM input

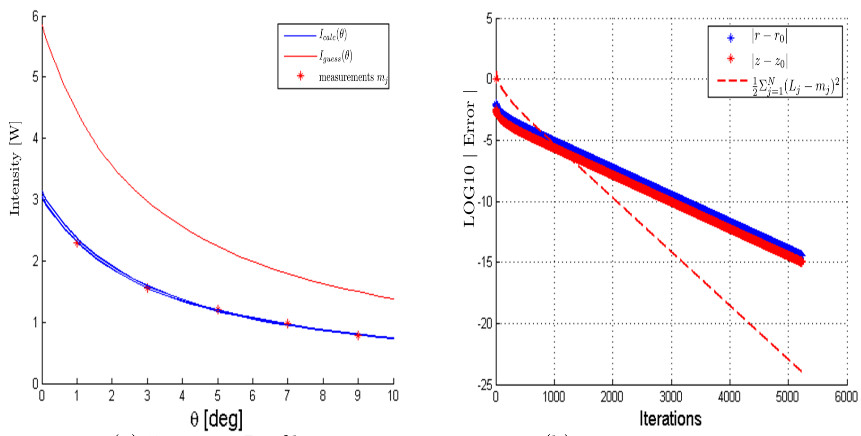

(a) Intensity Profile (b) Error over iterations

Figure 3.: Convergence results for shooting method

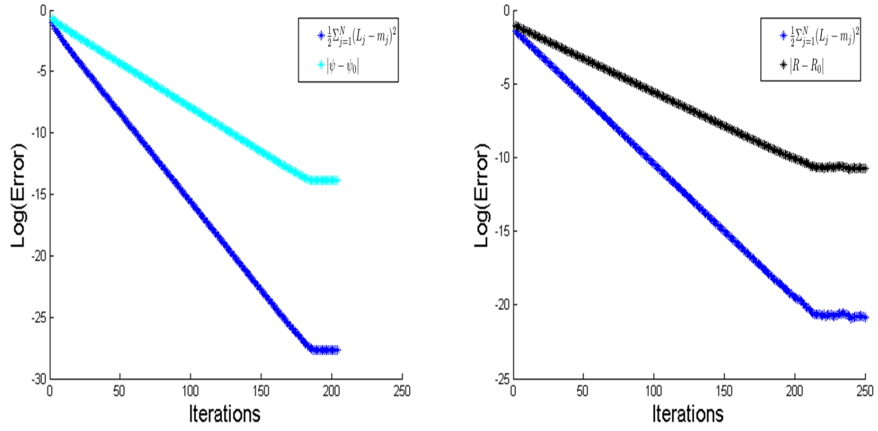

(a) ψ_0 unknown (b) R_0 unknown

Figure 4.: Convergence results for Newton's Method with one unknown.

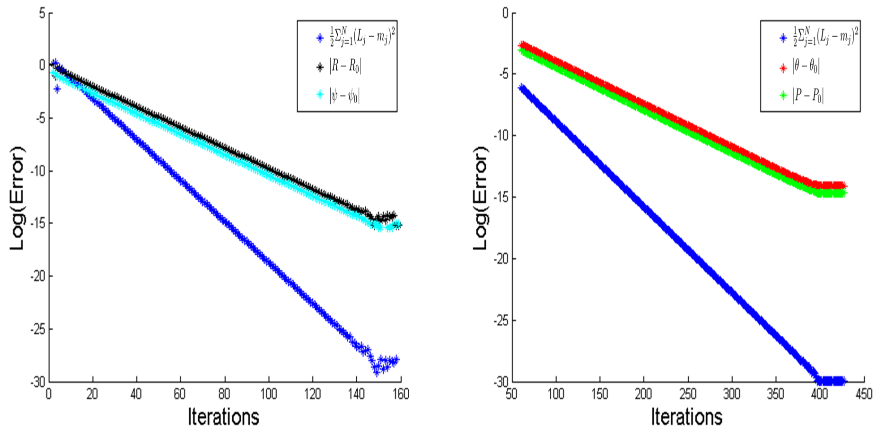

(a) (R_0, ψ_0) unknown (b) (θ_0, P_0) unknown

Figure 5.: Convergence results for Newton's Method with two unknowns.

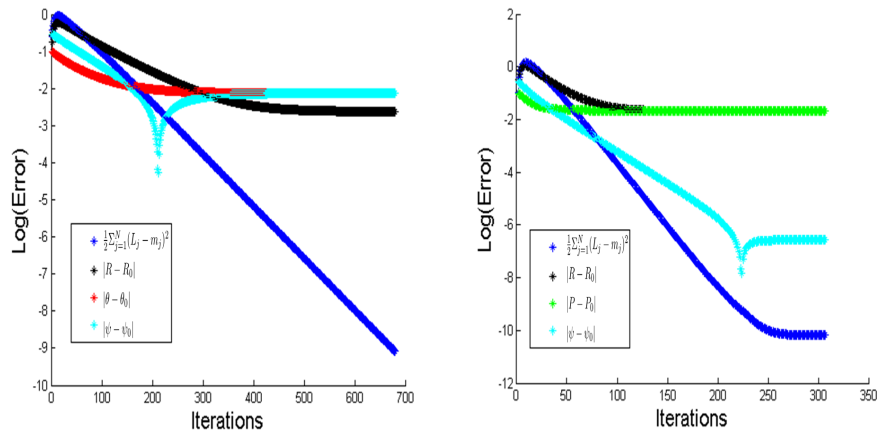

(a) (R_0, θ_0, ψ_0) unknown (b) (R_0, P_0, ψ_0) unknown

Figure 6.: Convergence results for Newton's Method with three unknowns.

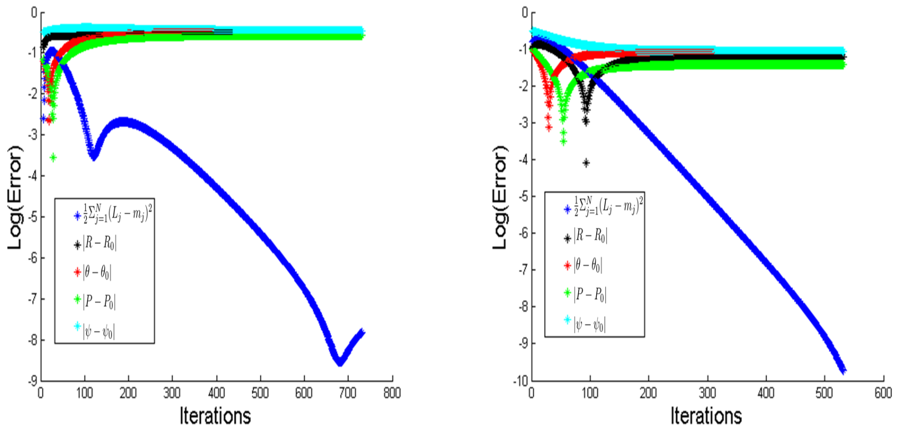

(a) $(R_0, \theta_0, P_0, \psi_0)$ unknown, 4 measurements (b) $(R_0, \theta_0, P_0, \psi_0)$ unknown, 6 measurements

Figure 7.: Convergence results for Newton's Method with four unknowns.

Quantity	Nominal Value	Variation	$\lvert R-R_0\rvert$	$\lvert P-P_0\rvert$	$\lvert\psi-\psi_0\rvert$	$\lvert\theta-\theta_0\rvert$
Wind Speed	2 m/s	$\{1.4, 1.7, 2, 2.3, 2.6\}$ m/s	1.51%	1.23%	1.11%	0.33°
Altitude	2 m	$\{1.4, 1.7, 2, 2.3, 2.6\}$ m	1.18 %	1.05%	0.88%	0.2651°
Relative Humidity	90%	$\{85, 87.5, 90, 92.5, 95\}$ %	1.54 %	0.47%	1.13%	0.34°
Air Mass Parameter	3	$\{2.4, 2.7, 3, 3.3, 3.6\}$	0.79%	0.59%	0.60%	0.18°

Table 2.: Simplex Method robustness with uncertain in ANAM paramters

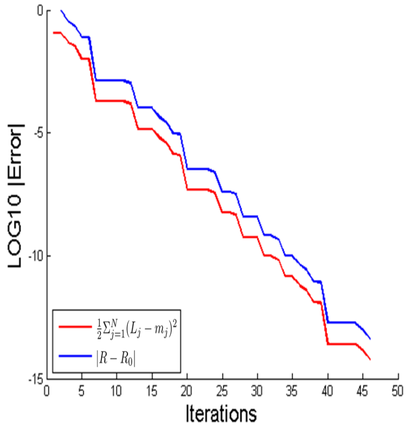

(a) R unknown

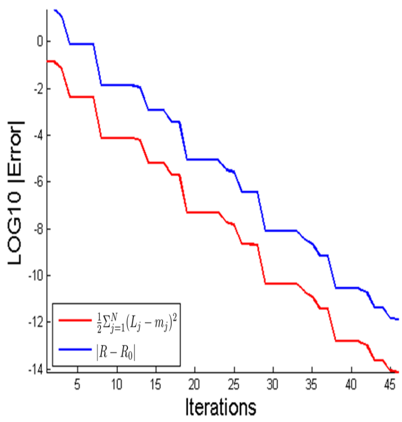

(b) P_0 unknown

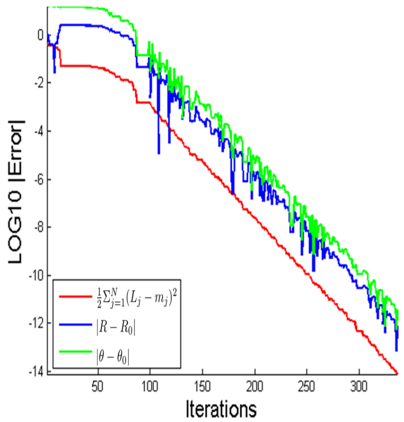

(c) (R, θ) unknown

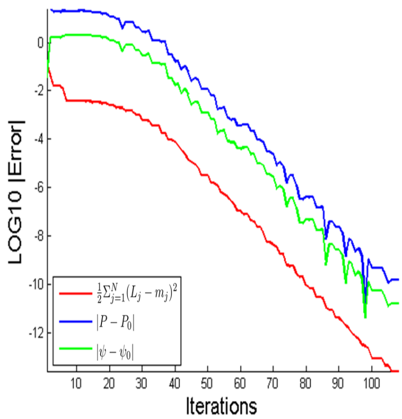

(d) (P_0, ψ) unknown

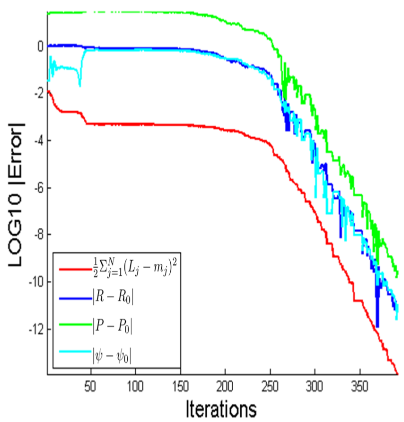

(e) (R, P_0, ψ) unknown

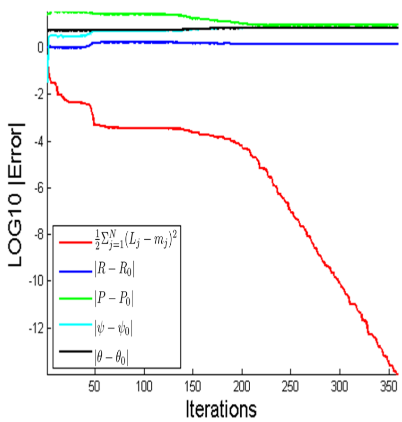

(f) (R, P_0, ψ, θ) unknown

Figure 8.: Convergence results for inversion of the scalar model using a simplex method.

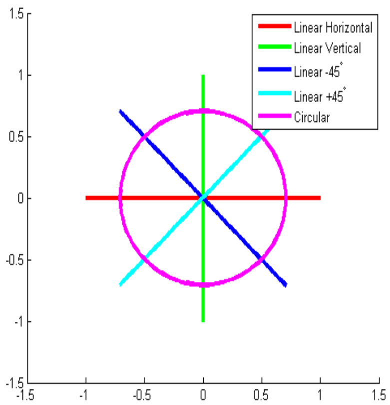

(a) Incident Stokes vectors

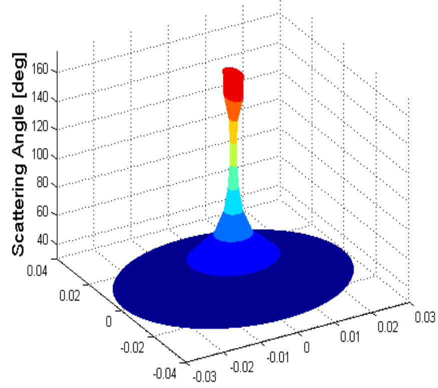

(b) Circularly polarized Mie scattering

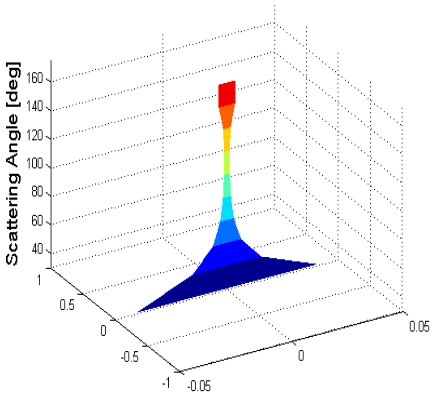

(c) Horizontally polarized Mie scattering

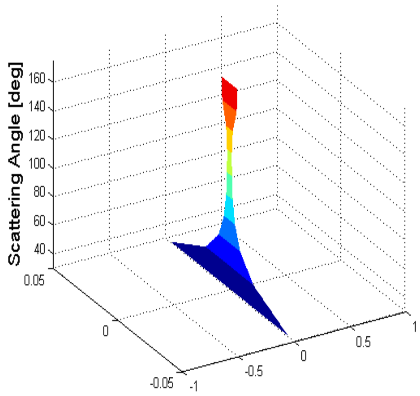

(d) Vertically polarized Mie scattering

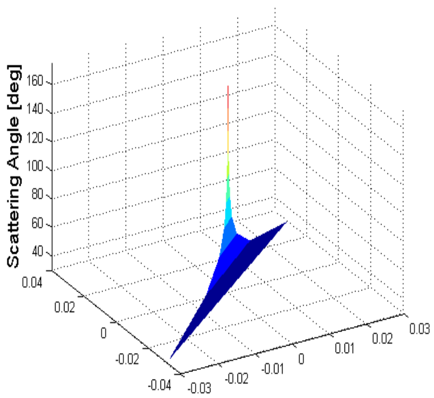

(e) $+45°$ polarized scattering

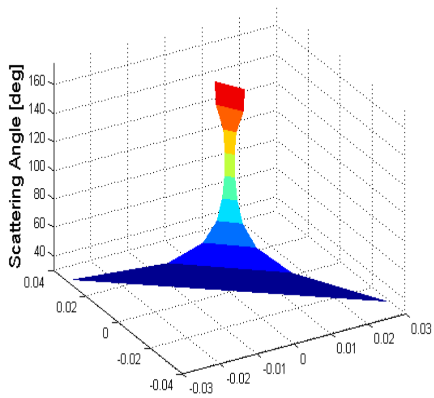

(f) $-45°$ polarized scattering

Figure 9.

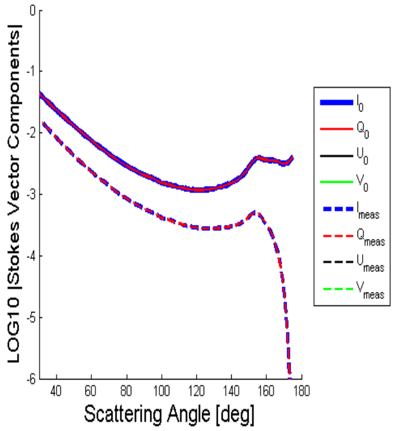

(a) Horizontally polarized scattering

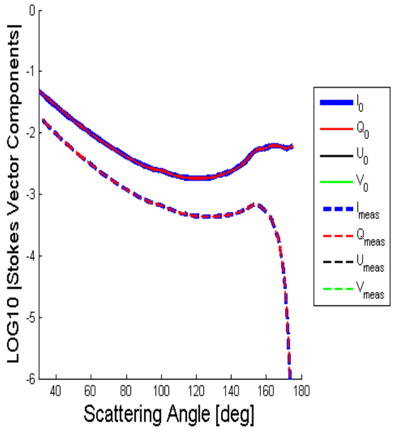

(b) Vertically polarized scattering

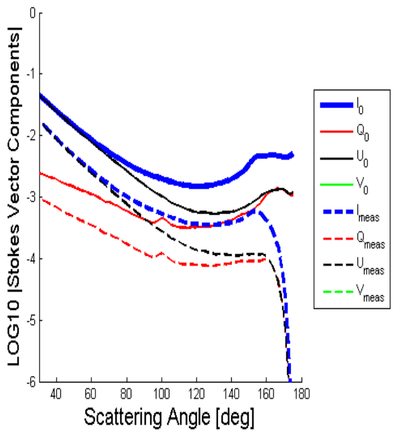

(c) $+45°$ polarized scattering

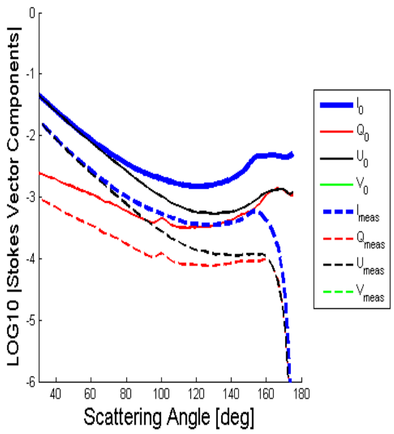

(d) $-45°$ polarized scattering

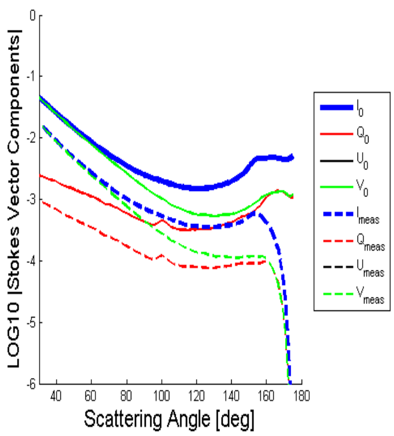

(e) RH Circularly polarized scattering

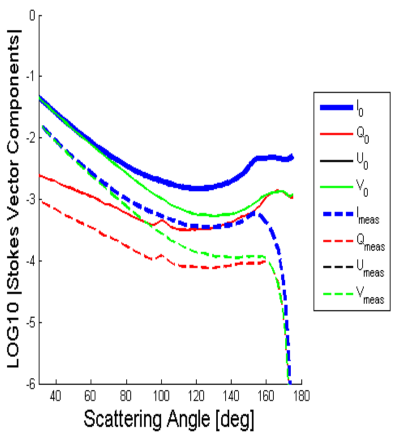

(f) LH Circularly polarized scattering

Figure 10.: Range = 5km, $\psi = 30°$

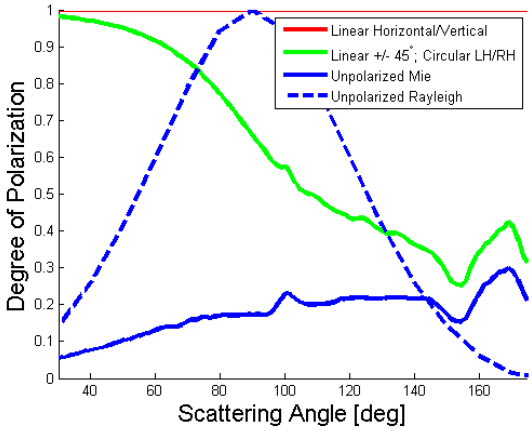

Figure 11.: Degree of polarization variation with scattering angle.
Range = 5km, $\psi = 30°$

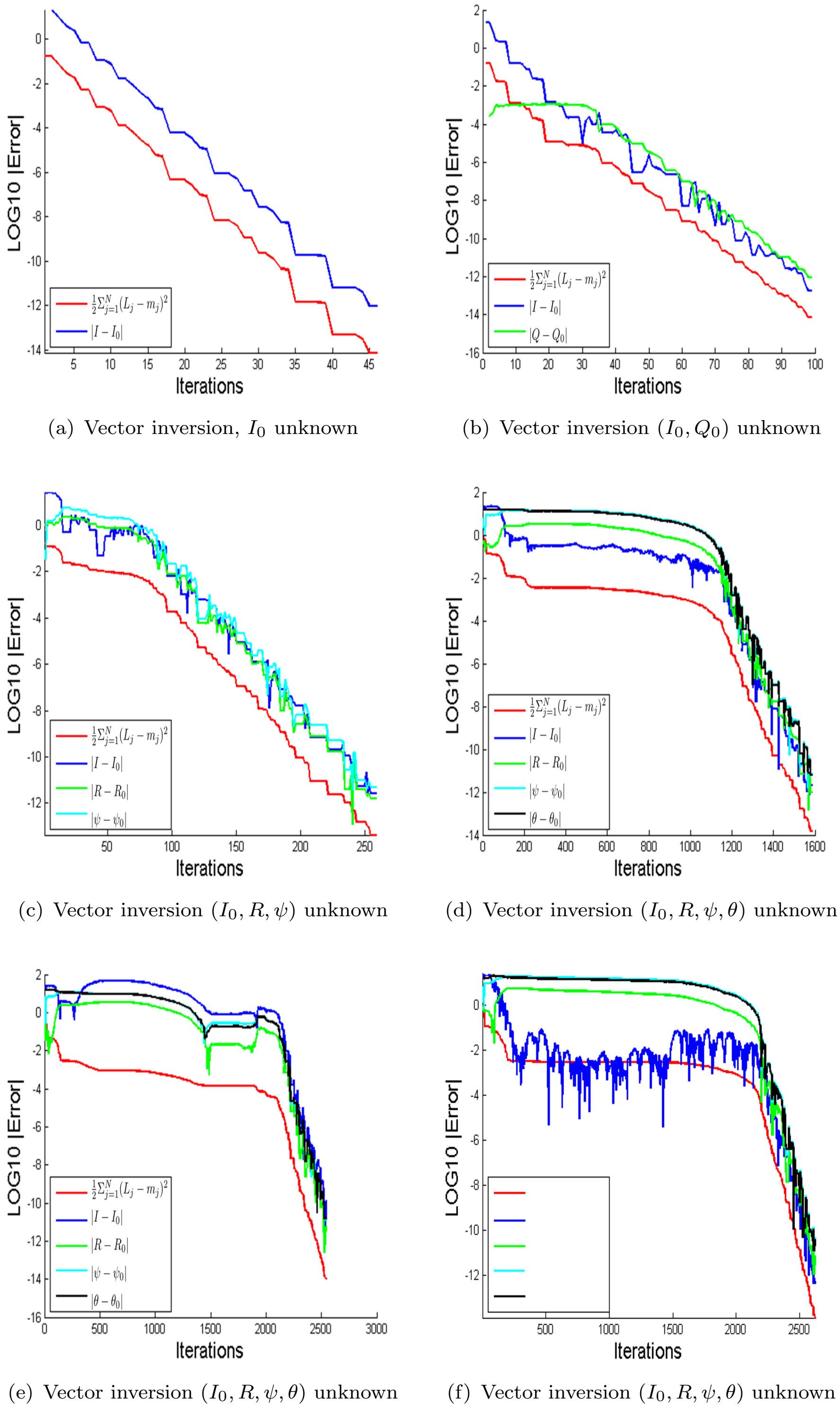

(a) Vector inversion, I_0 unknown

(b) Vector inversion (I_0, Q_0) unknown

(c) Vector inversion (I_0, R, ψ) unknown

(d) Vector inversion (I_0, R, ψ, θ) unknown

(e) Vector inversion (I_0, R, ψ, θ) unknown

(f) Vector inversion (I_0, R, ψ, θ) unknown

Figure 12.: Convergence results for inversion of the Stokes system using four measurements. (12.a-d) Circularly polarized incident light. (12.e) Un-polarized incident light. (12.f) Vertically polarized incident light.

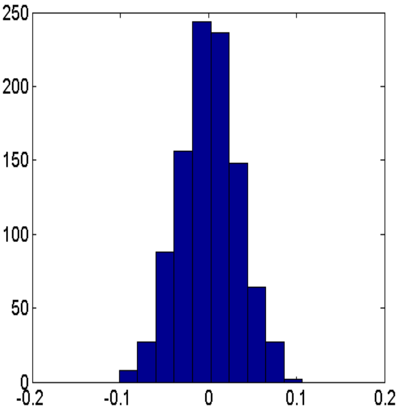

(a) Histogram of $R - R_0$, single unknown case, 1000 trials, SNR = 0.01

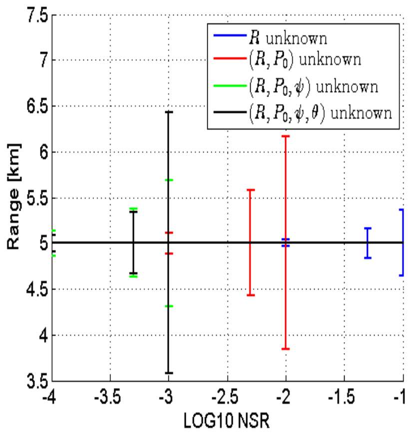

(b) Confidence intervals for R

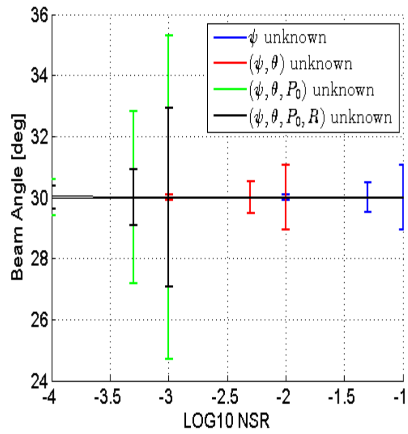

(c) Confidence intervals for ψ

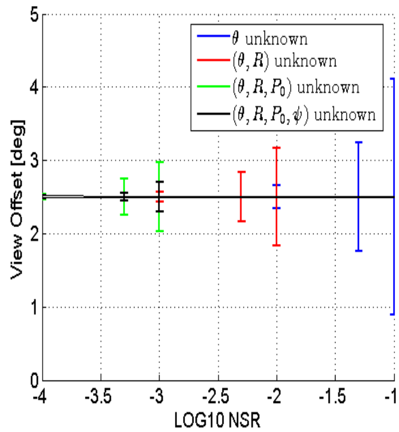

(d) Confidence intervals for θ

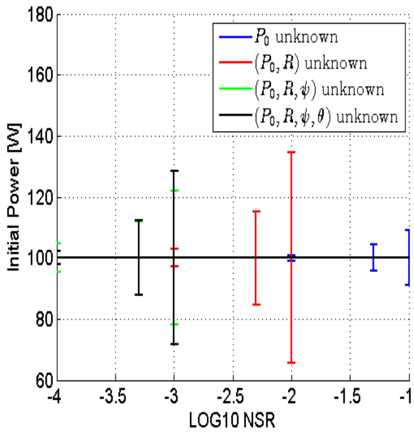

(e) Confidence intervals for P_0

Figure 13.: One standard deviation confidence intervals for parameter estimation with sensor noise.